Current Research in Microbial Sciences 10 (2026) 100571

Contents lists available at ScienceDirect

Current Research in Microbial Sciences

journal homepage: www.sciencedirect.com/journal/current-research-in-microbial-sciences

Layer-dependent modulation of *S. aureus* biofilms by light-induced oxidative stress

Kate C. Blanco [a,b,*], Paul de Figueiredo [c], Jace A. Willis [a], Leonardo De Boni [b], Letícia P. Martinelli [b], Vladislav V. Yakovlev [a], Vanderlei S. Bagnato [a,b]

[a] Department of Biomedical Engineering, Texas A&M University, College Station, TX 77840, USA
[b] São Carlos Institute of Physics, University of São Paulo, São Carlos 13566-590, Brazil
[c] College of Medicine, Texas A&M University, College Station, TX 77840, USA

ARTICLE INFO

Keywords:
S. aureus biofilms
Light-induced oxidative stress
Photodynamic effects
Layer-dependent responses
Post-treatment behavior
Biofilm modulation

ABSTRACT

Background: Bacterial biofilms display pronounced spatial heterogeneity, generating, yet how these effects are distributed across biofilm layers and how surviving cells respond after treatment remain poorly understood.
Methods: *Staphylococcus aureus* biofilms (S biofilm) were exposed to light-induced oxidative stress, and post-treatment responses were evaluated through growth kinetics, biofilm reformation capacity, and layer-dependent photosensitizer penetration. S biofilms with different maturation times and structural complexities were analyzed to assess how biofilm architecture modulates photosensitizer distribution across superficial and deeper regions.
Results: Light-induced oxidative stress altered post-treatment growth dynamics and impaired the ability of surviving cells to re-establish structured biofilms. Photosensitizer penetration was strongly layer-dependent and influenced by S biofilm maturation and complexity, resulting in spatially heterogeneous photodynamic effects. These effects differentially impacted cells located in superficial versus deeper biofilm regions.
Conclusion: These findings demonstrate that photodynamic treatment modulates S. aureus biofilm behavior in a layer-dependent manner, weakening protective niches without requiring complete eradication. By disrupting biofilm microenvironments associated with tolerance and persistence, light-induced oxidative stress limits biofilm recovery and provides a mechanistic basis for photodynamic strategies aimed at controlling biofilm re-establishment.

1. Introduction

Microbial biofilms are structured communities in which bacterial cells are embedded in a self-produced extracellular matrix, composed mainly of polysaccharides, proteins, lipids, and extracellular DNA (Costerton et al., 1999; Flemming and Wingender, 2010). Biofilm formation and maturation confer spatial organization and functional heterogeneity to the community, while establishing a microenvironment with limited diffusion, reducing the penetration of antimicrobial agents and significantly increasing tolerance compared to planktonic cells (Stewart and Costerton, 2001; Mah, 2012; Sharma et al., 2019).

The three-dimensional architecture of biofilms is closely associated with the formation of physicochemical gradients, especially of nutrients and oxygen, which shape the spatial distribution of bacterial physiological states (Stewart and Franklin, 2008; Borriello et al., 2004; Xu et al., 1998). Cells located in the surface layers tend to exhibit higher metabolic activity and growth rates, while populations located in deeper regions face nutritional limitation and hypoxia, favoring the transition to slow-growth or dormant states (Stewart, 2012; Xu et al., 1998). This physiological stratification constitutes a collective adaptive response that increases biofilm survival under environmental stress conditions (Flemming and Wingender, 2010; Stewart and Franklin, 2008). As a direct consequence of this organization, biofilms exhibit marked phenotypic heterogeneity, with dormant or slow-growing subpopulations showing reduced metabolism and increased tolerance to antimicrobial agents (Lewis, 2001, 2007). These persistent subpopulations play a central role in biofilm recurrence, acting as reservoirs capable of re-establishing the community after structural disruption induced by antimicrobial treatments (Wille and Coenye, 2020). Thus, biofilm persistence is not only due to the presence of the extracellular

* Corresponding author at: Texas A&M University, Emerging Technologies Building 3120, 101 Bizzell St, College Station, TX 77843, USA.
E-mail address: kateblanco@ifsc.usp.br (K.C. Blanco).

https://doi.org/10.1016/j.crmicr.2026.100571

Available online 18 February 2026

matrix, but also to the coexistence of distinct physiological states within the same structure (Lewis, 2007; Stewart, 2012).

In this context, photodynamic antimicrobial approaches emerge as promising strategies for biofilm control. Oxidative photodynamic therapy (PDT) is based on the activation of a photosensitizer by light in the presence of oxygen, leading to the generation of reactive oxygen species (ROS) capable of inducing oxidative damage to both microbial cells and the extracellular matrix of the biofilm (Hamblin and Hasan, 2004; Willis et al., 2021; Zangirolami et al., 2018). Unlike conventional antibiotics, the effects of PDT do not depend on specific molecular targets, reducing the likelihood of classical resistance (Cieplik et al., 2018; Maisch, 2015).

In addition to its direct cytotoxic effects, ROS generation is recognized as a spatially regulated process by the local availability of oxygen, redox balance, and microenvironmental constraints imposed by the biofilm architecture itself (Ge et al., 2025a, 2023, 2024). These factors modulate not only antimicrobial efficacy but also host-microorganism interactions and post-treatment recovery processes.

Although PDT is effective against biofilms, it remains poorly understood how light-induced oxidative stress is distributed across the different layers of the biofilm and how this distribution affects physiologically distinct subpopulations, especially surviving cells after treatment (Cieplik et al., 2018; Maisch, 2015). In particular, it is still unclear how oxygen-regulated redox processes modulate post-treatment physiology and influence biofilm persistence and recurrence (Ge et al., 2024,; 2025b; Ruan et al., 2025; Wainwright et al., 2017).

In this study, we demonstrate that light-induced oxidative stress acts in a depth-dependent manner in *Staphylococcus aureus biofilms,* modulating photosensitizer penetration and cellular behavior after treatment. By integrating biofilm maturation parameters, structural complexity, and photosensitizer incubation time, we show that PDT promotes the spatial redistribution of oxidative stress, compromising microenvironments traditionally associated with antimicrobial tolerance. These effects result in impaired biofilm structural integrity and limited functional recovery, providing a mechanistic basis for understanding how photodynamic approaches weaken biofilm persistence beyond direct microbial elimination. Although multispecies biofilms are widespread, this study focuses exclusively on multistrain *Staphylococcus aureus* biofilms as a Gram-positive model system, and the conclusions are restricted to this context.

2. Materials and methods

2.1. Microrganisms

Staphylococcus aureus was used as the model organism in this study. The strains included *S. aureus* ATCC 25,925, a methicillin-resistant *S. aureus* strains (MRSA) and USA300 ATCC TCH1516, USA300-HOU-MR. These strains were selected to evaluate photodynamically induced oxidative stress in both planktonic cultures and S biofilm models. Bacterial stocks were stored at −80 °C in Brain Heart Infusion (BHI) broth supplemented with glycerol (final concentration 40 % v/v). For experiments, frozen stocks were thawed and inoculated into fresh BHI broth. Pre-inoculum cultures were prepared by incubating 1 mL of bacterial suspension in 9 mL of BHI broth at 37 ± 0.1 °C under orbital shaking (150–200 rpm) for 16 h.

2.2. Biofilm models

2.2.1. Biofilm formation and post-PDT remnant cells

Cells from pre-inoculum cultures were harvested by centrifugation, washed twice with phosphate-buffered saline (PBS), and centrifuged at 5000 rpm for 15 min. S biofilms were formed by inoculating 10 % (v/v) of the bacterial suspension (initial concentration of 1×10^8 CFU·mL^{-1}) into fresh BHI broth. Aliquots were transferred to multiwell plates (1000 μL per well) and confocal dishes (100 μL per dish). Bacterial suspensions were homogenized by repeated pipetting prior to incubation to ensure uniform cell distribution.

S biofilms were allowed to develop under static conditions at 37 °C for either 24 h or 48 h, with culture medium replaced every 24 h to sustain biofilm growth. Based on species composition and maturation time, biofilms were classified as follows: X1 and X2 correspond to single-species *Staphylococcus aureus* biofilms formed for 24 h and 48 h, respectively, whereas XY1 and XY2 represent two-strain *S* biofilms formed for 24 h and 48 h. These conditions were used to generate biofilms with increasing maturation and structural complexity. After formation, biofilms were characterized by determination of colony-forming units (CFU·mL^{-1}) and subsequently used for treatment and post-treatment analyses.

2.2.2. Growth kinetics

To evaluate post-treatment physiological responses, surviving cells from planktonic and S biofilm cultures subjected to photodynamic inactivation (Section 2.2) were recovered and analyzed for growth kinetics. Three independent colonies per condition were randomly selected from BHI agar plates after 24 h incubation at 37 °C and inoculated into fresh BHI broth. Cultures were incubated at 37 °C under agitation, and 100 μL aliquots were collected at 60 min intervals for a total period of 16 h. Optical density was measured at 660 nm using a UV–Vis spectrophotometer with a 1 cm path length. Growth curves were analyzed to assess changes in lag phase duration and exponential growth behavior following photodynamic exposure.

2.2.3. Antibiotic time-kill assay

Time–kill assays were performed to quantify the survival dynamics of *Staphylococcus aureus* strains under antibiotic exposure. S biofilm cultures formed for 48 h were disrupted, diluted in fresh BHI broth, and adjusted to an initial density of approximately 1×10^6 CFU·mL^{-1}. Aliquots were distributed into sterile tubes and exposed to antibiotics under aerobic conditions at 37 °C with orbital shaking. For *S. aureus* ATCC 25,925, methicillin and oxacillin were tested; for *S. aureus* USA300 ATCC TCH1516, amoxicillin and oxacillin were tested. At predetermined time points (0, 5, 10, 15, and 20 min), samples were collected, immediately serially diluted in PBS, and plated on BHI agar for CFU enumeration. Plates were incubated at 37 °C for 24 h prior to counting. Survival was expressed as $\log_{10}$(CFU·mL^{-1}) as a function of exposure time. Data represent mean values with standard deviation from independent biological replicates ($n \geq 3$).

2.3. Photodynamic inactivation

Photodynamic inactivation experiments were performed using four experimental groups: untreated control (bacteria only), dark control (bacteria + photosensitizer), light control (bacteria + light), and photodynamic treatment (bacteria + photosensitizer + light). This experimental design enabled discrimination between photochemical effects and those associated exclusively with light exposure or photosensitizer incubation. For dark and photodynamic groups, bacterial suspensions were incubated with curcumin at a final concentration of 5 mM, prepared from a stock solution in absolute ethanol, resulting in a final ethanol concentration of 10 % (v/v). Dark controls containing the same ethanol concentration were included to exclude solvent-related effects. Photosensitizer incubation was performed for 15 min under dark conditions to allow interaction with bacterial cells. Light and photodynamic groups were irradiated with blue light (450 nm) at an irradiance of 70 mW·cm^{-2}, delivering total radiant exposures of 40 or 80 J·cm^{-2}. These light doses were selected to induce different levels of oxidative stress and to evaluate post-treatment microbial responses. After treatment, bacterial suspensions were serially diluted and plated on BHI agar for determination of colony-forming units (CFU·mL^{-1}). Optical density at 660 nm was measured in parallel to assess bulk changes in microbial growth.

2.3.1. Multiple cycles

To assess S biofilm recovery following repeated oxidative stress, biofilms subjected to photodynamic treatment were gently rinsed with 1 mL of PBS for 1 min to remove planktonic cells and non-adherent material. Remaining adhered biofilm cells were re-incubated under biofilm-forming conditions for 24 h. Photodynamic treatment was applied for up to three cycles, with 24 h intervals between cycles, corresponding to a total incubation period of 48 h. After each cycle, biofilm formation capacity was evaluated as described above, enabling analysis of biofilm persistence and re-establishment following successive oxidative stress events.

2.4. Spectrophotometric analysis of curcumin photoconversion

UV–Vis spectrophotometric analyses were performed to evaluate light-induced photoconversion and consumption of curcumin under different experimental conditions. For experiments corresponding to Figure S2, absorption spectra were acquired using a conventional UV–Vis spectrophotometer. A curcumin stock solution (5 mM) was prepared in absolute ethanol and diluted as required for spectral acquisition. Spectra were recorded over the wavelength range of 200–800 nm at 1 min intervals during continuous blue-light illumination (450 nm), corresponding to increasing radiant exposures. The absorption spectrum recorded prior to illumination (0 min) was used as a reference for intact curcumin. Progressive spectral changes, including attenuation of the characteristic absorption band centered at ~425 nm and the emergence of features at shorter wavelengths (~360 nm), were monitored as a function of illumination time. For experiments corresponding to Figure S3, spectrophotometric measurements were performed using a Multiskan GO microplate reader (Thermo Fisher Scientific, USA). Experiments were conducted in clear-bottom 96-well microplates with a final volume of 400 µL per well. Curcumin was added to all experimental groups at a final working concentration of 5 µM, prepared by dilution of the 5 mM stock solution. The following conditions were analyzed: curcumin in culture medium alone, culture medium with curcumin in the presence of a mature (48 h) *S* biofilm, and curcumin-only controls. Absorption spectra were acquired individually for each well over the wavelength range of 300–1000 nm with a spectral resolution of 1 nm using SkanIt RE software (version 7.1). Spectra obtained from wells containing culture medium with curcumin but without bacterial cells were used as the baseline and subtracted from spectra acquired in the presence of biofilms to account for medium-related absorption contributions. Measurements were performed before irradiation (0 min) and after 3, 6, 9, 13, and 26 min of light exposure. Irradiation was carried out at 450 nm, corresponding to a total delivered radiant exposure of 80 $J \cdot cm^{-2}$. For each time point, absorption spectra were averaged across technical replicates, and data are presented as mean values with standard deviation.

2.5. Confocal microscopy

Confocal imaging was performed using an Olympus Fluoview 3000 confocal microscope coupled to an inverted IX83 microscope equipped with a second-generation zero-drift compensator (IX3-ZDC2). Images were acquired using a 60 × PlanApo oil immersion objective (numerical aperture 1.4). Excitation was provided by solid-state diode lasers at 405 and 488 nm. Laser power and acquisition parameters were kept constant across experimental conditions to allow comparative analyses while minimizing photobleaching and signal saturation. Layer segmentation and quantitative image analysis are described in detail in the Supplementary Information.

2.6. Statistical analyses

Statistical analyses were performed to evaluate differences in microbial growth kinetics and S biofilm formation capacity following photodynamic treatment. Data were analyzed using one-way analysis of variance (ANOVA). When significant differences were detected, pairwise comparisons were performed using Student's *t*-test. All analyses were conducted using Qtiplot software (version 5.9.8), and results were considered statistically significant at $p \leq 0.05$. All experiments were performed with at least three independent biological replicates ($n \geq 3$).

3. Results

3.1. Post-treatment growth dynamics

Growth kinetics were analyzed to assess the physiological response of *Staphylococcus aureus* cells surviving light-induced oxidative stress. Surviving cells from planktonic cultures and S biofilm-derived populations were re-incubated under optimal growth conditions and compared with untreated and dark controls (Fig. 1a,b).

Photodynamic treatment induced a clear delay in growth onset relative to controls. In both planktonic and S biofilm-derived populations, exposure to 80 $J \cdot cm^{-2}$ resulted in an extended lag phase of approximately 2 h. This effect was more pronounced in biofilm-derived cells, which also displayed reduced optical density increase during the exponential growth phase (Fig. 1b). Quantitative analysis of cumulative growth, estimated from the area under the optical density curves over 16 h (Fig. 2), revealed a dose-dependent impairment in post-treatment populations. Biofilm-derived cells exposed to 80 $J \cdot cm^{-2}$ exhibited the strongest reduction in cumulative growth compared to planktonic cells. Together, these results indicate that light-induced oxidative stress not only delays growth initiation but also compromises the growth capacity of surviving cells, under standard culture conditions, particularly those originating from biofilms.

To increase biological complexity while maintaining a controlled experimental system, biofilms composed of multiple Staphylococcus aureus strains were evaluated. The selected strains exhibit distinct growth kinetics and tolerance profiles, allowing assessment of how intra-species heterogeneity influences post-photodynamic recovery and biofilm re-establishment. This multi-strain approach preserves species-specific structural and physiological features while introducing competitive and cooperative interactions that modulate biofilm organization and recovery dynamics.

3.2. S biofilm recovery following repeated photodynamic treatment

The impact of repeated photodynamic treatment on biofilm recovery was evaluated over three consecutive sessions, with bacterial regrowth assessed 24 h after each treatment cycle. Biofilm-associated cells of *S. aureus*, MRSA, and mixed (*S. aureus* + MRSA) biofilms were quantified as $\log(CFU \cdot mL^{-1})$ and compared across untreated, light-only, dark, and photodynamic conditions (Fig. 2). Successive photodynamic treatments progressively impaired biofilm recovery, resulting in reduced bacterial counts relative to controls. In monospecies biofilms, a more pronounced reduction in recoverable *S. aureus* cells was observed, whereas mixed biofilms exhibited increased cellular dispersion and reduced structural reformation. Notably, repeated photodynamic exposure prevented biofilms from returning to their original structural organization, indicating a cumulative disruption of biofilm resilience following successive oxidative stress events.

3.3. Layer-dependent curcumin penetration in early-stage S biofilms

S biofilms exhibited a spatially heterogeneous organization that enabled evaluation of curcumin distribution across defined biofilm layers. As illustrated in the schematic representation (Fig. 3a–c), biofilms were segmented into four analytical layers extending from the biofilm–medium interface (layer 1) to the region adjacent to the substratum (layer 4). To assess layer-dependent penetration, curcumin localization was analyzed in single-species *Staphylococcus aureus*

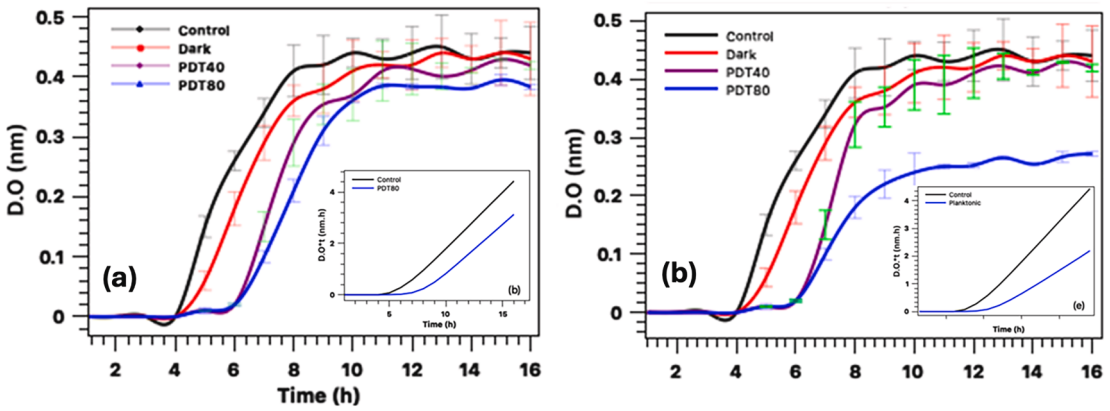

Fig. 1. Growth kinetics of *Staphylococcus aureus* populations surviving photodynamic treatment. Growth curves of planktonic cultures (a) and *S. aureus* biofilm-derived cells (b) exposed to light-induced oxidative stress at 40 J·cm^{-2} (purple) and 80 J·cm^{-2} (blue) are shown in comparison with untreated controls (black) and dark controls (red). The light-only control (bacteria + light, without curcumin) did not differ from the untreated control under the conditions tested and is therefore not shown separately. Insets within each panel, displayed in lighter color tones, represent the same optical density data plotted on a reduced scale and were used for quantitative analysis of cumulative growth over the 16 h incubation period.

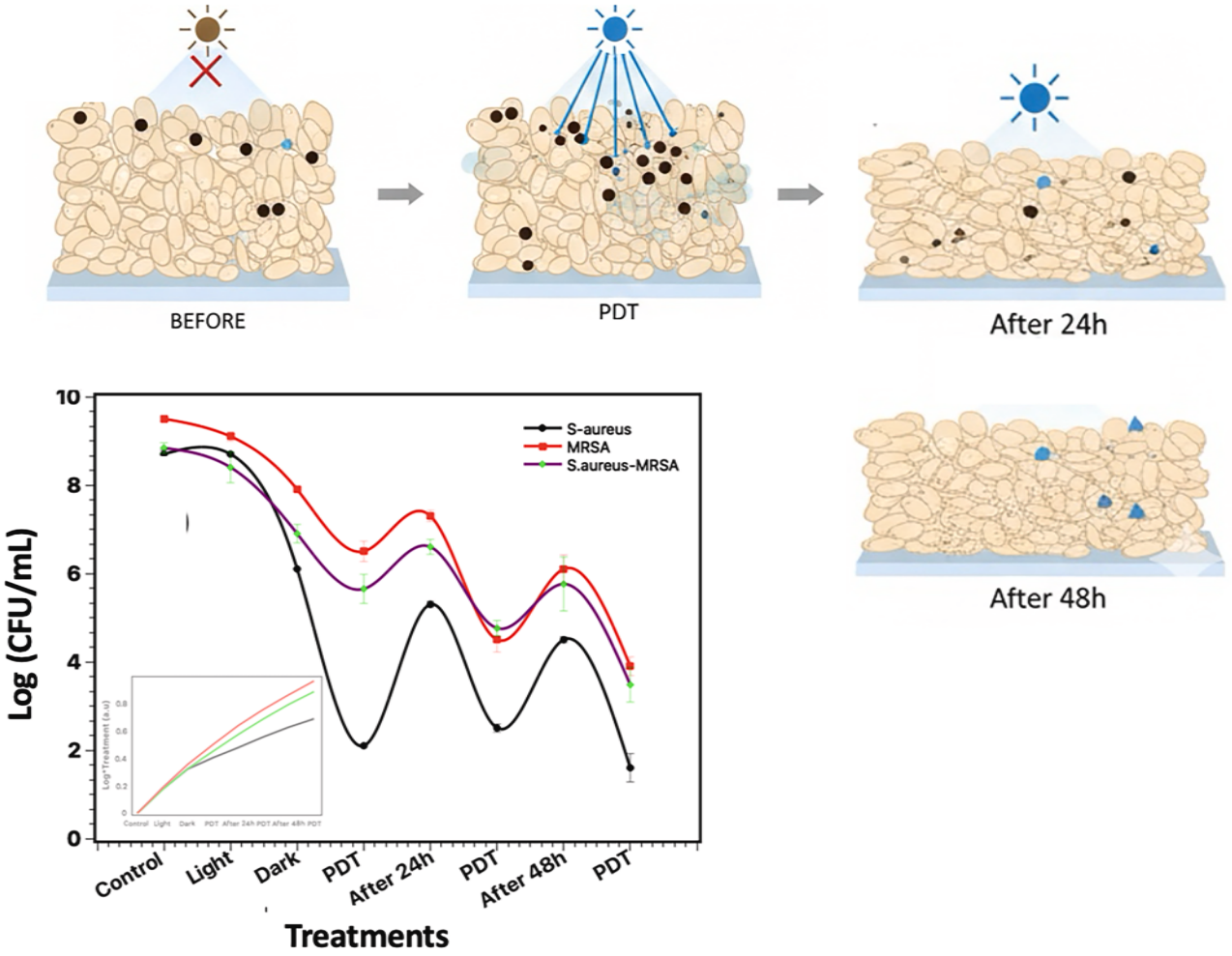

Fig. 2. Growth and biofilm recovery dynamics of mono-strain and multi-strain *Staphylococcus aureus* biofilms following photodynamic treatment. Multi-strain biofilms were composed exclusively of *S. aureus* lineages with distinct physiological profiles, serving as a model of intra-species heterogeneity rather than poly-microbial or multispecies communities.

biofilms formed under shorter maturation conditions. Confocal fluorescence images corresponding to each analytical layer were acquired according to the layer definition shown in Fig. 3b Curcumin penetration was not uniform across the biofilm structure. After 5 min of incubation, fluorescence was predominantly detected in the superficial and intermediate layers (layers 1 and 2), whereas deeper layers (layers 3 and 4) exhibited limited signal (Fig. 3d–g). After 45 min of incubation, curcumin fluorescence extended into deeper layers (layers 3 and 4), indicating

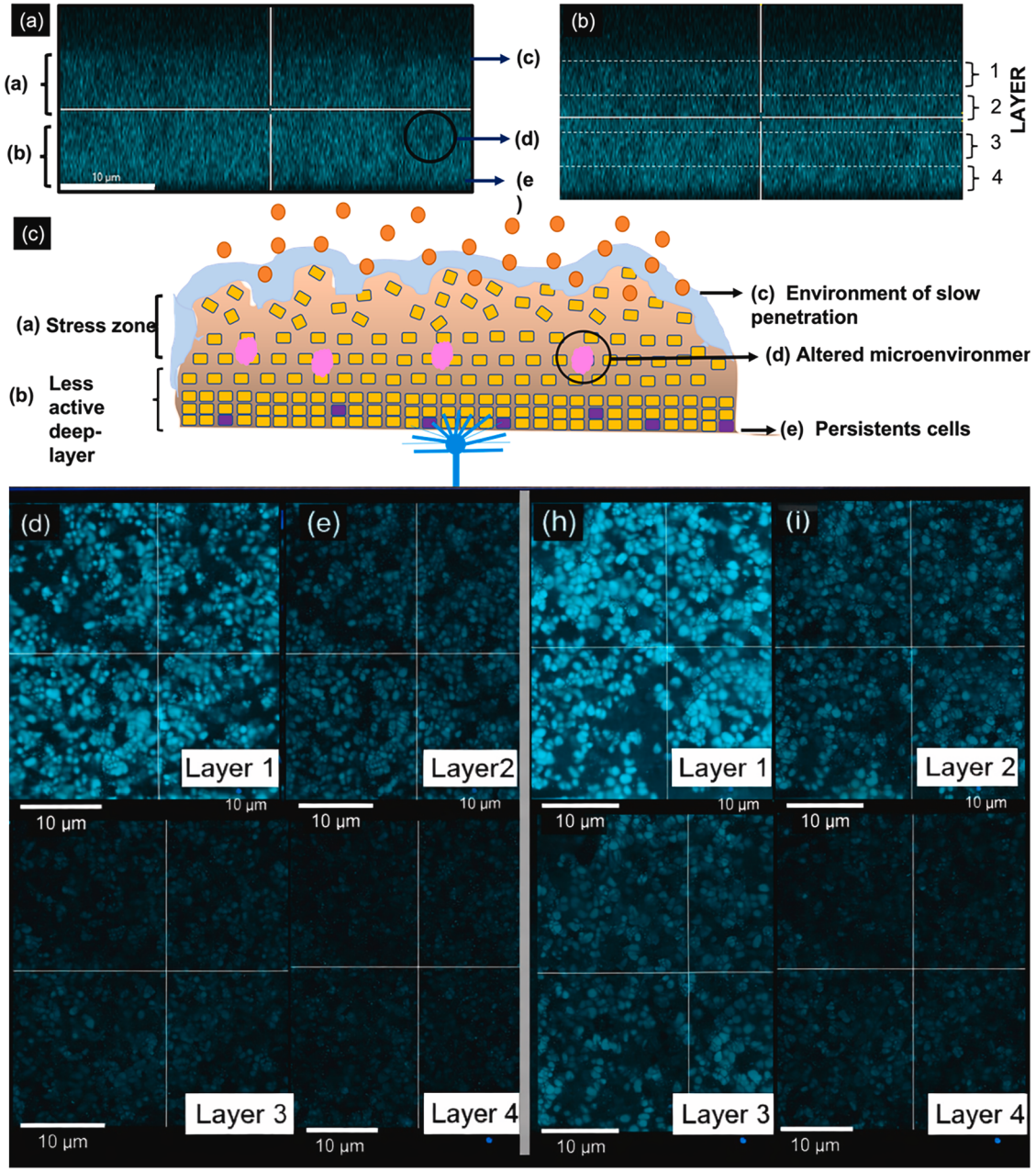

Fig. 3. Schematic representation of biofilm organization and analytical layer definition. (a) Representative biofilm regions highlighting the biofilm–medium and biofilm–substratum interfaces. (b) Definition of four analytical biofilm layers (layers 1–4) used for fluorescence analysis. (c) Conceptual illustration of curcumin distribution and light exposure within the biofilm structure. (d–g) Confocal fluorescence images showing curcumin localization across layers 1–4 after 5 min of incubation. (h–k) Corresponding images after 45 min of incubation in early-stage single-species *Staphylococcus aureus* biofilms.

time-dependent diffusion through the biofilm matrix (Fig. 3h–k). These results demonstrate that curcumin distribution within biofilms depends on both incubation time and biofilm depth, even in early-stage biofilms, highlighting that spatial heterogeneity emerges prior to full biofilm maturation.

3.4. Structural modulation and layer-dependent curcumin distribution

Photodynamic treatment induced structural alterations within the S biofilm architecture, evidenced by changes in porosity across specific biofilm layers. Confocal fluorescence analysis revealed the formation of porous regions following photodynamic exposure, predominantly within layer 2, as defined in the schematic representation of biofilm organization.

Layer 2, located immediately below the biofilm surface and corresponding to the transition zone between superficial and deeper layers, exhibited localized prolonged curcumin incubation partially restored porosity after photodynamic treatment. This effect was observed both in early-stage single-strain biofilms and in more complex two-strain biofilms formed under longer maturation conditions (Fig. 4a,b). Quantitative porosity analysis showed that increasing biofilm maturation time and structural complexity reduced the extent of porosity formation following short curcumin incubation. In contrast, prolonged curcumin incubation partially restored porosity across different biofilm architectures, indicating a time-dependent interaction between curcumin diffusion and biofilm structure (Fig. 4c). To further characterize curcumin distribution, fluorescence intensity was quantified across the four analytical layers defined in Fig. 3b S biofilms formed under shorter

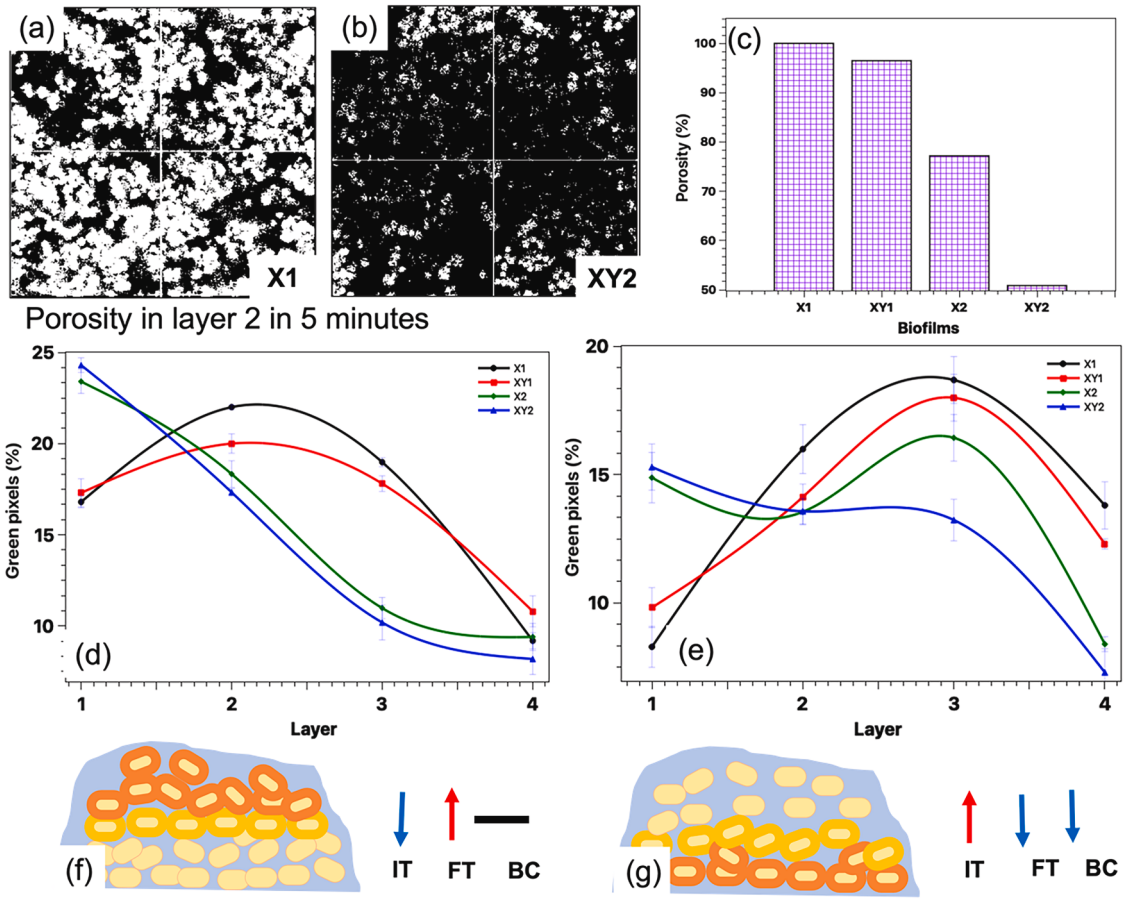

Fig. 4. Photodynamic-induced structural and penetration changes within bacterial S biofilms. (a,b) Confocal images showing porous regions formed in S biofilm layer 2 after photodynamic treatment in single-species and two-strain *Staphylococcus aureus* biofilms formed under different maturation conditions. (c) Quantification of biofilm porosity for single-species and two-strain biofilms formed under shorter and longer maturation times after 45 min of curcumin incubation. (d,e) Quantification of curcumin fluorescence intensity (green pixels) across S biofilm layers 1–4 after 5 min (d) and 45 min (e) of incubation. (f,g) Schematic representation summarizing observed trends in curcumin distribution across superficial (layers 1–2) and deeper (layers 3–4) S biofilm regions as a function of incubation time, S biofilm maturation, and S biofilm complexity.

maturation times exhibited higher curcumin incorporation in superficial layers (layers 1 and 2) after 5 min of incubation (Fig. 4d). After 45 min of incubation, increased fluorescence signal was detected in deeper layers, particularly layer 3, indicating enhanced penetration with prolonged incubation (Fig. 4e). Overall, increasing biofilm maturation reduced curcumin incorporation during short incubation periods, whereas longer incubation resulted in a more homogeneous distribution across layers 1–3. These results demonstrate that curcumin penetration and photodynamic-induced structural modulation are jointly influenced by incubation time, biofilm maturation, and biofilm structural complexity.

4. Discussion

This study employed *Staphylococcus aureus* biofilms as a Gram-positive model system, including mono-strain and dual-strain (*S. aureus-S. aureus*) biofilms. Accordingly, the layer-dependent photodynamic effects described here should be interpreted as species-specific and not directly extrapolated to Gram-negative bacteria or complex polymicrobial biofilms.

Our results demonstrate that antimicrobial PDT induces sustained alterations in bacterial physiology that extends beyond immediate microbial inactivation. Rather than acting solely as an acute bactericidal insult, light-induced oxidative stress reshapes post-treatment bacterial behavior, particularly in biofilm-associated populations. This is evidenced by delayed growth onset, reduced cumulative growth, and impaired biofilm re-establishment under otherwise optimal growth conditions following PDT exposure (Fig. 2a,b), indicating limited adaptive recovery (Ikhimiukor et al., 2022; Imlay, 2013).

The growth delay observed in both planktonic and biofilm-derived *S. aureus* populations (Fig. 2a) suggests disruption of cellular processes required for efficient cell cycle progression. Although nutrient availability is a fundamental determinant of bacterial growth, the reduced post-PDT growth rates indicate that impaired metabolic capacity, rather than nutrient limitation alone, underlies this response. ROS generated during PDT oxidize proteins, lipids, and nucleic acids, thereby compromising enzymatic activity, central metabolic pathways, and regulatory networks governing DNA replication, transcription, and cell division (Farr and Kogoma, 1991; Imlay, 2013). Such oxidative damage provides a mechanistic explanation for the prolonged lag phase and reduced exponential growth efficiency observed in surviving cells.

Layer-resolved fluorescence analysis revealed a heterogeneous distribution of curcumin across biofilm depth (Fig. 3d–k), demonstrating that photosensitizer availability is strongly modulated by incubation time and biofilm architecture. Because ROS generation during PDT scales with the product of photosensitizer concentration, light irradiance, and oxygen availability, spatial variations in curcumin localization directly constrain where oxidative stress can be generated. In this context, fluorescence intensity serves as a semi-quantitative proxy for relative ROS generation potential, reflecting spatial differences in oxidative burden rather than absolute ROS levels, as irradiation parameters were held constant across experimental conditions (Gordon and Schneider, 2012; Priyadarsini, 2014).

Independent spectroscopic measurements further support curcumin photoactivation during illumination. The progressive decrease of the characteristic absorption band at ~425 nm, accompanied by the emergence of a new band around ~360 nm (Fig. 1c), indicates curcumin consumption and photoproduct formation (Gordon and Schneider, 2012; Priyadarsini, 2014). This light-dependent chemical conversion confirms active photochemical reactions consistent with ROS generation, reinforcing the interpretation of spatially heterogeneous oxidative stress without implying direct measurement of ROS gradients.

From a mechanistic perspective, curcumin differs from many classical porphyrin-based photosensitizers by predominantly operating through Type I photochemical pathways, generating short-lived radical species such as superoxide, hydrogen peroxide, and hydroxyl radicals (Dias et al., 2020). Given the limited diffusion distances and high reactivity of these species, oxidative stress is expected to remain highly localized and strongly dependent on the spatial coupling between photosensitizer availability, light penetration, and oxygen microgradients (Ge et al., 2023, 2024; Gordon and Schneider, 2012; Priyadarsini, 2014). This localization is consistent with the non-uniform fluorescence profiles observed across biofilm layers (Fig. 3).

Beyond direct intracellular damage, PDT-induced ROS also generates extracellular oxidative and osmotic stress signals within the biofilm matrix. In biofilms, where cells exist in heterogeneous physiological states and remain interconnected through chemical signaling, such perturbations may propagate across the community, amplifying post-treatment effects and influencing antimicrobial immune accessibility (Flemming and Wingender, 2010; Ge et al., 2024; Ruan et al., 2025; Stewart, 2012). The structural disruptions observed after PDT, including altered biofilm density and porosity (Fig. 3c), support this community-level impact.

PDT effects were not uniform across biofilm depth but were strongly layer-dependent . Biofilms exhibit pronounced metabolic stratification driven by nutrient and oxygen gradients, with metabolically active cells predominating near the biofilm surface and slow-growing or dormant cells enriched in deeper regions (Stewart and Franklin, 2008; Xu et al., 1998). Because ROS have limited lifetimes and diffusion ranges, their biological impact is intrinsically linked to photosensitizer localization. Consistent with this framework, curcumin preferentially accumulated in superficial and intermediate layers during short incubation times, resulting in higher oxidative stress in these regions (Fig. 3d,e, h,i), while deeper layers remained partially shielded, particularly in mature and structurally complex biofilms (Fig. 3f,g, j,k).

Although fluorescence intensity is often assumed to be highest at the biofilm surface due to direct exposure and diffusion attenuation, this assumption does not necessarily hold for mature biofilms treated with diffusible photosensitizers. In such systems, fluorescence intensity reflects the combined influence of photosensitizer penetration, retention within the extracellular matrix, and biofilm architectural heterogeneity. Accordingly, layer-resolved fluorescence analysis was employed to capture non-monotonic spatial distributions of photosensitizer signals arising from these physicochemical constraints. The substantial fluorescence observed in intermediate layers (Fig. 3e,i) indicates localized accumulation and retention rather than simple surface-limited diffusion, providing insight into spatially heterogeneous oxidative stress generation during PDT.

Oxidative disruption of the extracellular polymeric substance matrix further altered biofilm architecture in a spatially heterogeneous manner. The formation of PDT-induced porosity in intermediate layers (Fig. 3c) likely reduced local cohesiveness, transiently increasing permeability and facilitating limited propagation of oxidative effects. However, increased biofilm maturation and matrix density restricted both photosensitizer penetration and ROS diffusion, necessitating prolonged incubation to achieve broader curcumin distribution and structural impact (Flemming et al., 2016; Wille and Coenye, 2020).

Numerous studies demonstrate that biofilms exhibit spatial stratification in metabolic activity, with slow-growing or persistent -like subpopulations enriched in deeper regions (Bjarnsholt et al., 2013; Lewis, 2007; Stewart and Franklin, 2008; Xu et al., 1998). Time–kill analyzes further support the presence of functional heterogeneity at the population level. The biphasic killing profiles observed (Supplementary Figure S1) are characteristic of heterogeneous bacterial populations composed of rapidly killed susceptible cells and slower-killed tolerant or persistent-like subpopulations (Brauner et al., 2016; Lewis, 2007; Balaban et al., 2019). These assays are consistent with established associations between tolerant phenotypes and biofilm regions characterized by limited oxygen and nutrient diffusion.

Repeated PDT exposure further reduced biofilm reformation capacity. Although recolonization was still observed, biofilm biomass remained consistently lower after multiple PDT cycles (Fig. 2c), indicating incomplete recovery. This cumulative effect likely arises from repeated structural disruption combined with sustained metabolic impairment, preventing full restoration of protective biofilm microenvironments.

Beyond incubation-dependent modulation of photosensitizer penetration, physical strategies that transiently disrupt biofilm architecture may further enhance photodynamic efficacy. Ultrasound pre-treatment has been shown to partially loosen the extracellular polymeric substance matrix, increase biofilm permeability, and facilitate antimicrobial and photosensitizer diffusion without necessarily causing direct bacterial killing. Within this framework, ultrasound-assisted pre-treatment prior to curcumin incubation represents a rational complementary strategy to enhance photosensitizer distribution and promote more homogeneous ROS generation. Although ultrasound was not employed in the present study, the penetration-based mechanisms identified here (Figs. 1–3) provide a clear mechanistic rationale for such combination approaches, which will be explored in future investigations.

Collectively, these findings support a conceptual framework in which PDT functions primarily as a biofilm modulation strategy rather than a standalone eradication approach. Spatially heterogeneous photosensitizer distribution (Fig. 3), localized ROS generation (Fig. 1), and layer-dependent structural alterations weaken protective biofilm niches without uniformly eliminating all bacterial cells. By reducing diffusion barriers, altering local tolerance states, and exposing previously protected subpopulations, PDT creates transient windows of increased vulnerability that can be exploited by sequential combination strategies, such as PDT followed by antibiotic treatment or immune-mediated clearance. This spatially informed perspective provides a mechanistic basis for optimizing PDT protocols aimed at destabilizing biofilm-associated persistence and limiting recurrence (Figs. 2 and S1) (Brauner et al., 2016; Ge et al., 2024, 2025a).

5. Conclusions

This study demonstrates that antimicrobial PDT affects bacterial behavior beyond immediate microbial inactivation, inducing persistent alterations in post-treatment growth dynamics and S biofilm re-establishment capacity. Surviving cells exhibited delayed growth onset, reduced cumulative growth, and impaired ability to rebuild structured biofilms, indicating that PDT modulates cellular physiology and community organization rather than acting solely as a bactericidal approach.

The observed effects were influenced by biofilm architecture and curcumin CUR penetration across distinct biofilm layers. Layer-dependent CUR distribution revealed that light-induced oxidative stress is spatially heterogeneous within biofilms and depends on incubation time, biofilm maturation, and structural complexity. These factors directly impact the extent to which PDT disrupts biofilm integrity and limits post-treatment recovery.

By altering regions traditionally associated with reduced antimicrobial penetration, PDT was shown to weaken the protective biofilm microenvironments that favor persistence and recurrence of infection. Although complete eradication was not always achieved, repeated

photodynamic exposure maintained bacterial populations at reduced levels and limited biofilm reformation, suggesting a potential role for PDT as a strategy to control biofilm-associated infections.

Overall, these findings highlight the importance of considering biofilm heterogeneity, treatment timing, and photosensitizer penetration when designing PDT-based antimicrobial protocols. The ability of light-induced oxidative stress to modulate post-treatment bacterial behavior and biofilm organization provides a mechanistic basis for optimizing PDT as an adjunct approach in the management of complex and persistent infections.

CRediT authorship contribution statement

Kate C. Blanco: Conceptualization, Methodology, Investigation, Formal analysis, Writing – original draft, Writing – review & editing. **Paul de Figueiredo:** Methodology, Investigation. **Jace A. Willis:** Methodology, Investigation. **Leonardo De Boni:** Methodology, Formal analysis. **Letícia P. Martinelli:** Methodology, Investigation, Data curation. **Vladislav V. Yakovlev:** Writing – original draft, Supervision. **Vanderlei S. Bagnato:** Funding acquisition, Supervision, Resources, Writing – review & editing.

Declaration of competing interest

The authors declare the following financial interests/personal relationships which may be considered as potential competing interests:

Kate Blanco reports financial support was provided by University of São Paulo and Texas A&M University. Kate Blanco reports a relationship with State of São Paulo Research Foundation and Vanderlei Bagnato with the Cancer Prevention and Research Institute of Texas, that includes: If there are other authors, they declare that they have no known competing financial interests or personal relationships that could have appeared to influence the work reported in this paper.

Acknowledgments

The authors acknowledge financial support from the São Paulo Research Foundation (FAPESP) and the Texas Institute for Cancer Prevention and Research. Kate Blanco acknowledges FAPESP postdoctoral fellowship 2019/12694-3 and BEPE-FAPESP 2021/09952-0, and Vanderlei Bagnato acknowledges CPRIT Scholar in Cancer Research (RR220054). This article also received financial support from the Governor's University Research Initiative and the Chancellor's Research Initiative.

Supplementary materials

Supplementary material associated with this article can be found, in the online version, at doi:10.1016/j.crmicr.2026.100571.

References

Balaban, N.Q., Helaine, S., Lewis, K., et al., 2019. Definitions and guidelines for research on antibiotic persistence. Nat. Rev. Microbiol. 17, 441–448.
Bjarnsholt, T., Jensen, P.Ø., Fiandaca, M.J., et al., 2013. Pseudomonas aeruginosa biofilms in the respiratory tract of cystic fibrosis patients. Pediatr. Pulmonol. 44, 547–558.
Borriello, G., Werner, E., Roe, F., et al., 2004. Oxygen limitation contributes to antibiotic tolerance of Pseudomonas aeruginosa in biofilms. Antimicrob. Agents Chemother. 48, 2659–2664.
Brauner, A., Fridman, O., Gefen, O., Balaban, N.Q., 2016. Distinguishing between resistance, tolerance and persistence to antibiotic treatment. Nat. Rev. Microbiol. 14, 320–330.
Cieplik, F., Buchalla, W., Hellwig, E., Al-Ahmad, A., Hiller, K.A., Maisch, T., 2018. Antimicrobial photodynamic therapy as an adjunct for treatment of biofilm infections. Periodontol. 2000 76, 83–96.
Costerton, J.W., Stewart, P.S., Greenberg, E.P., 1999. Bacterial biofilms: a common cause of persistent infections. Science 284, 1318–1322.
Dias, L.D., Blanco, K.C., Bagnato, V.S., 2020. Mechanisms of antimicrobial photodynamic therapy mediated by curcumin. Photodiagn. Photodyn. Ther. 31, 101892.
Farr, S.B., Kogoma, T., 1991. Oxidative stress responses in Escherichia coli and Salmonella typhimurium. Microbiol. Rev. 55, 561–585.
Flemming, H.C., Neu, T.R., Wozniak, D.J., 2016. The EPS matrix: the "house of biofilm cells. J. Bacteriol. 198, 1653–1660.
Flemming, H.C., Wingender, J., 2010. The biofilm matrix. Nat. Rev. Microbiol. 8, 623–633.
Ge, M., Guo, Z., Ruan, Z., et al., 2025a. Chemical substrate-enabled piezoelectric metabolic reprogramming therapy unlocks the vicious triad of diabetic wounds. Cell Biomater., 100276
Ge, M., Guo, H., Zong, M., Chen, Z., Liu, Z., Lin, H., Shi, J., 2023. Bandgap-engineered germanene nanosheets as an efficient photodynamic agent for cancer therapy. Angew. Chem. Int. Ed. 62, e202215795.
Ge, M., Mei, J., Hu, T., Yang, C., Lin, H., Shi, J., 2025b. Piezoelectric-enhanced nanocatalysts trigger neutrophil N1 polarization against bacterial biofilm by disrupting redox homeostasis. Adv. Mater. 37, 2409633.
Ge, M., Zhu, Y.X., Ruan, Z., et al., 2024. A natural killer cell mimic against intracellular pathogen infections. Sci. Adv. 10, eadp3976.
Gordon, R., Schneider, E., 2012. Photodegradation pathways of curcumin. J. Phys. Chem. A 116, 6598–6605.
Hamblin, M.R., Hasan, T., 2004. Photodynamic therapy: a new antimicrobial approach to infectious disease? Photochem. Photobiol. Sci. 3, 436–450.
Ikhimiukor, O.O., Odih, E.E., Donado-Godoy, P., Okeke, I.N., 2022. A bottom-up view of antimicrobial resistance transmission in developing countries. Nat. Microbiol. 7, 757–765.
Imlay, J.A., 2013. The molecular mechanisms and physiological consequences of oxidative stress. Annu. Rev. Microbiol. 67, 181–203.
Lewis, K., 2001. Riddle of biofilm resistance. Antimicrob. Agents Chemother. 45, 999–1007.
Lewis, K., 2007. Persister cells, dormancy and infectious disease. Nat. Rev. Microbiol. 5, 48–56.
Mah, T.F., 2012. Biofilm-specific antibiotic resistance. Fut. Microbiol. 7, 1061–1072.
Maisch, T., 2015. Resistance in antimicrobial photodynamic inactivation of bacteria. Photochem. Photobiol. Sci. 14, 1518–1526.
Priyadarsini, K.I., 2014. The chemistry of curcumin: from extraction to therapeutic agent. Molecules 19, 20091–20112.
Ruan, Z., Shi, T., Guo, Z., et al., 2025. Oxygen-immunomodulated nanocatalysts enhance anti-infection by trained immunity. Adv. Funct. Mater., e09454
Sharma, D., Misba, L., Khan, A.U., 2019. Antibiotics versus biofilm: an emerging battleground in microbial communities. Antimicrob. Resist. Infect. Control 8, 76.
Stewart, P.S., 2012. Mini-review: convection around biofilms. Biofouling 28, 187–198.
Stewart, P.S., Costerton, J.W., 2001. Antibiotic resistance of bacteria in biofilms. Lancet 358, 135–138.
Stewart, P.S., Franklin, M.J., 2008. Physiological heterogeneity in biofilms. Nat. Rev. Microbiol. 6, 199–210.
Wainwright, M., Maisch, T., Nonell, S., et al., 2017. Photoantimicrobials—are we afraid of the light? Lancet Infect. Dis. 17, e49–e55.
Wille, J., Coenye, T., 2020. Biofilm dispersion: the key to biofilm eradication or opening Pandora's box? Biofilm 2, 100027.
Willis, J.A., Cheburkanov, V., Kassab, G., Soares, J.M., Blanco, K.C., Bagnato, V.S., Yakovlev, V.V., 2021. Photodynamic viral inactivation: recent advances and potential applications. Appl. Phys. Rev. 8, 021315.
Xu, K.D., Stewart, P.S., Xia, F., Huang, C.T., McFeters, G.A., 1998. Spatial physiological heterogeneity in Pseudomonas aeruginosa biofilm is determined by oxygen availability. Appl. Environ. Microbiol. 64, 4035–4039.
Zangirolami, A.C., Inada, N.M., Bagnato, V.S., Blanco, K.C., 2018. Biofilm destruction on endotracheal tubes by photodynamic inactivation. Infect. Disord. Drug Targ. 18, 128–135.